Transformation of Long Surface and Tsunami-Like Waves in the Ocean with a Variable Bathymetry

A. M. Ermakov[1] and Y. A. Stepanyants[1,2]

Abstract—We consider a transformation of long linear waves in an ocean with a variable depth. We calculate the transformation coefficients (the coefficients of transmission and reflection) as the functions of frequency and the total depth drop for three typical models of bottom profile variation: (i) piecewise-linear, (ii) piecewise-quadratic, and (iii) hyperbolic tangent profiles. For all these cases, exact solutions are obtained, analysed and graphically illustrated. This allows us to derive the transformation coefficients in the analytic form for the subsequent comparison with the results of approximate, numerical, or experimental study. We show that the results obtained are in agreement with both the energy flux conservation and Lamb's formulae in the limiting case of zero frequency. We also study wave transformation on the underwater barriers and trenches of different shapes and compare the results obtained.

Key words: Shallow water, tsunami wave, variable bathymetry, wave transformation.

1. Introduction

The problem of linear wave transformation on the bottom unevenness has a long history. The development of rigorous mathematical methods for the description of wave transformation in the coastal zone represents an important and topical problem from both the academic and practical points of view, especially in application to the protection of marine engineering constructions (platforms, gas and oil pipelines, etc.) (Belibassakis et al. 2017) and coastlines against hazardous impacts of large oceanic waves including tsunami waves (Harris and Vila-Concejo 2013; Ferrario et al. 2014). As is well-known (see, for example, Pelinovsky 1996; Levin and Nosov 2009), tsunami waves in the open ocean can be treated in the same way as the linear waves in a shallow basin; their typical heights are about 0.5 m, and wavelengths are 300–500 km, whereas the average ocean depth is 4–5 km. Therefore, scattering of such waves on underwater mountain ranges or trenches can be studied within the framework of linear shallow water theory. Figure 1 from https://en.wikipedia.org/wiki/Continental_shelf illustrates schematically the continental slope located between the shelf where the depth varies linearly in average and continental foot, bordering the ocean bed. According to https://en.wikipedia.org/wiki/Continental_shelf, in the continental slope the depth varies greatly and can be approximates either by a linear function or quadratic function as shown in Fig. 1. The typical variation of the bottom angle is from about 3°–4° to 40°–45° and even more. The average bottom slope is about 3.5°, which is close to the slope of the mountain ranges. The continental slope covers a significant range of depths, in general, from 100–200 m to 3000–4000 m and has a typical width from 300 km up to 2000 km. This make the problem of wave transformation in the ocean with a variable bathymetry very topical.

The problem of wave propagation in the fluid with uneven bottom has a general solution in two limiting cases. When the bottom smoothly varies with the distance so that the characteristic scale of bottom variation is much greater than the wavelength, then the traditional JWKB method can be used to calculate wave parameters (amplitude, wavelength, and other parameters) (see, e.g., Massel 1989; Pelinovsky 1996; Dingemans 1997). In another limiting case when there is an underwater step-wise obstacle, the solution

[1] Faculty of Health, Engineering and Sciences, University of Southern Queensland, Toowoomba, QLD 4350, Australia. E-mail: ErmakovAndreiM@gmail.com; Yury.Stepanyants@usq.edu.au
[2] Department of Applied Mathematics, Nizhny Novgorod State Technical University, Nizhny Novgorod, Russia 603950.
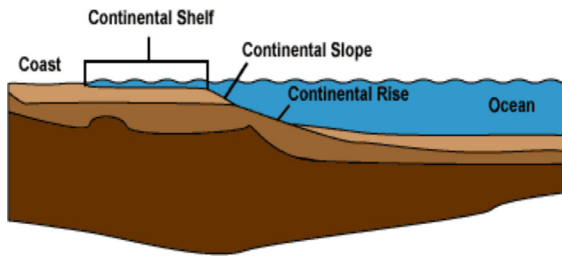
Figure 1
(Color figure online) A sketch of the typical oceanic profile (https://en.wikipedia.org/wiki/Continental_shelf)

for a wave field can be obtained on both sides from the step and then the solution can be matched at the boundary of two homogeneous regions. This procedure is not so trivial as may seem at first glance, because in general one should take into account not only travelling waves, but also the infinite series of evanescent modes (see Kurkin et al. 2015 and references therein). However, in the long-wave approximation contribution of evanescent modes into the wave scattering is negligible which significantly simplifies the problem (Dingemans 1997).

Besides these limiting cases the problem of long wave propagation can be solved analytically for some particular bottom profiles (Dean 1964; Mei 1990; Kânoğlu and Synolakis 1998; Jung et al. 2008; Xie et al. 2011) (see also Dingemans 1997), moreover for the linear bottom profile there is an exact solution of linearised hydrodynamic equations for waves of *arbitrary* wavelength (Stoker 1957; Sretenskii 1977). It has also been shown that in some particular cases exact solutions can be obtained for the reflectionless propagation of long linear and nonlinear waves in a fluid with a special bottom profiles (see Didenkulova and Pelinovsky 2013, 2016 and references therein).

Here we revise the problem of linear wave transformation in shallow water with three particular bottom profiles: (i) piecewise-linear, (ii) piecewise-quadratic, and (iii) hyperbolic tangent (tanh-) profiles. We show that in these particular cases the basic equations can be solved analytically and solutions can be presented in general in terms of hypergeometric functions, which can be reduced to elementary functions in particular cases. This allows us to derive the transformation coefficient and compare the results for all three profiles. Then we study wave transformation over underwater obstacles/trenches of finite

width, present the results in the graphical forms, and analyse them. Our consideration is confined to the normal incidence of waves on the plane (one-dimensional) underwater obstacles. As is well-known the effect of wave transmission is the greatest in this case. Therefore, the wave impact on a coastal zone and marine engineering constructions is the most dangerous at the normal incidence.

The main goal of this publication is to draw readers' attention to the possibility of construction of exact analytical solutions to the problem of water wave transformation on rather typical bottom profiles and demonstrate what is common and what is the different in the transformation coefficients. In a separate publication, we plan to present a more detailed analysis of wave transformation in basins with the typical bottom configurations and compare the theoretical results with the data of laboratory and numerical experiments. The results obtained are applicable not only to long surface waves (swell, wind waves) in the coastal zones, but also to tsunami waves in the open oceans where such waves are essentially linear. Scattering of tsunami waves on underwater mountain ranges and canyons is a topical problem, and results obtained allow one to estimate the amplitude of transmitted wave without the detail and costly numerical modelling, but using simple analytic formulae.

2. The Piecewise-Linear Bottom Profile

Consider first long linear surface wave scattering when it propagates in water with the piecewise-linear bottom profile shown in Fig. 2. An exact analytical solution to this problem was obtained by Dean (1964) as early as the beginning of 1960's (see also the book by Dingemans 1997 where other approaches to this problem are described). We shall re-consider this problem and present the results obtained in a form suitable for the comparison with other results derived for the parabolic and tanh-profiles. In the long-wave approximation the basic hydrodynamic equations representing mass and momentum conservations are (Carrier and Greenspan 1958):

$$\eta_t^* + [U(\eta^* + h)]_x = 0, \tag{1}$$
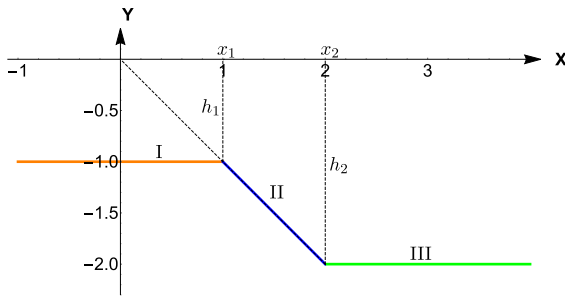
Figure 2
(Color figure online). A basin with the piecewise-linear bottom profile

$$g\eta_x^* + U_t + UU_x = 0, \qquad (2)$$

where U is the depth averaged fluid velocity, η^* is the perturbation of a free surface, g is the acceleration due to gravity, and h is the water depth. We assume that the water depth is constant, $h = h_1$ when $x \leq x_1$ and $h = h_2$ when $x \geq x_2$; in the interval $x_1 \leq x \leq x_2$ the depth changes linearly $h = \alpha x$ (see Fig. 2).

For the further analysis it is convenient to present the set of Eqs. (1) and (2) in the dimensionless form using the following change of variables:

$$V = \frac{U}{U_0}, \quad \eta = \frac{\eta^*}{\alpha l_0}, \quad \xi = \frac{x}{l_0}, \quad \hat{h} = \frac{h}{\alpha l_0} = \xi, \quad \hat{\omega} = \omega T, \qquad (3)$$

where $l_0 = x_2 - x_1$ (see Fig. 2), $T = l_0/\alpha g$, and $U_0 = (\alpha g l_0)^{1/2}$.

In the dimensionless variables the basic set of equations is:

$$\eta_\tau = -[V(\eta + h)]_\xi, \qquad (4)$$

$$\eta_\xi = -V_\tau - VV_\xi. \qquad (5)$$

Assuming that $\eta \ll h$, we obtain after linearisation and elimination of η the following wave equation:

$$V_{\tau\tau} - (Vh)_{\xi\xi} = 0. \qquad (6)$$

In the intervals where the fluid depth is constant, i.e., for $x < x_1$ and $x > x_2$, an elementary solution to this equation can be sought in the form $V \sim e^{i(\hat{\omega}\tau \pm k\xi)}$. However in the interval where the bottom linearly varies, i.e., when $x_1 < x < x_2$ and the depth $h = \xi$ in the dimensionless variables, the solution should be sought in the form: $V = \Psi(\xi)e^{i\hat{\omega}\tau}$. After substitution of this solution into Eq. (6) we obtain:

$$\xi\Psi_{\xi\xi} + 2\Psi_\xi + \hat{\omega}^2\Psi = 0. \qquad (7)$$

This is the standard Bessel equation whose solution is a linear combination of Bessel functions. Therefore for function $V(\xi, \tau)$ we obtain:

$$V(\xi) = \frac{1}{\hat{\omega}\sqrt{\xi}}\left[B_1 J_1(2\hat{\omega}\sqrt{\xi}) + B_2 Y_1(2\hat{\omega}\sqrt{\xi})\right]e^{i\hat{\omega}\tau}, \qquad (8)$$

where $J_1(x)$ and $Y_1(x)$ are Bessel functions of the first and second kinds respectively. Then in the linear approximation we find from Eq. (4) for $\eta = \Phi(\xi)e^{i\hat{\omega}\tau}$, where

$$\Phi(\xi) = \frac{i}{\hat{\omega}}\left[B_1 J_0(2\hat{\omega}\sqrt{\xi}) + B_2 Y_0(2\hat{\omega}\sqrt{\xi})\right]. \qquad (9)$$

Here $J_0(x)$ and $Y_0(x)$ are Bessel functions of the first and second kinds, but with zero indices.

Now we can write down the general solutions for the perturbation of a free surface in three different domains shown in Fig. 2:

$$\Phi_l = A_1 e^{-ik_1(\xi - \xi_1)} + A_2 e^{ik_1(\xi - \xi_1)}, \quad \xi \leq \xi_1; \qquad (10)$$

$$\Phi_c = \frac{i}{\hat{\omega}}\left[B_1 J_0(2\hat{\omega}\sqrt{\xi}) + B_2 Y_0(2\hat{\omega}\sqrt{\xi})\right], \quad \xi_1 \leq \xi \leq \xi_2; \qquad (11)$$

$$\Phi_r = C_1 e^{-ik_2(\xi - \xi_2)} + C_2 e^{ik_2(\xi - \xi_2)}, \quad \xi \geq \xi_2. \qquad (12)$$

where the wave numbers are

$$k_1 = \frac{\omega l_0}{\sqrt{gh_1}} = \frac{\hat{\omega}}{\sqrt{\xi_1}}, \quad k_2 = \frac{\omega l_0}{\sqrt{gh_2}} = \frac{\hat{\omega}}{\sqrt{\xi_2}}, \qquad (13)$$

and $A_{1,2}, B_{1,2}, C_{1,2}$ are arbitrary constants. Note that in stationary inhomogeneous media a wave frequency is conserved in the process of wave transformation.

Solutions (10)–(12) can be matched at the boundaries of domains 1, 2 and 3 shown in Fig. 2 by means of the following boundary conditions reflecting the continuity of function $\Phi(\xi)$ and its first derivative:

$$\Phi_l(\xi_1) = \Phi_c(\xi_1), \quad \Phi_c(\xi_2) = \Phi_r(\xi_2),$$
$$\Phi_l'(\xi_1) = \Phi_c'(\xi_1), \quad \Phi_c'(\xi_2) = \Phi_r'(\xi_2). \qquad (14)$$

Using these boundary conditions, we consider below surface wave transformation on the bottom unevenness when the incident wave arrives from the left and from the right.

2.1. Wave Transformation in the Case of Decreasing Depth

This case corresponds to the situation when an incident wave arrives from the right in Fig. 2. Then we set the following coefficients in the solutions (10)–(12):

$$A_1 = 0, \quad A_2 = T_r, \quad C_1 = R, \quad C_2 = 1, \quad (15)$$

where C_2 is the amplitude of an incident wave, R is the reflection coefficient (the amplitude of reflected wave), and T_r is the transmission coefficient (the amplitude of transmitted wave).

By substitution solutions (10)–(12) with the coefficients (15) into the boundary conditions (14), we obtain the transformation coefficients R and T, as well as the expressions for the wave amplitudes B_1 and B_2 in the transient region II (see Fig. 2):

$$
\begin{aligned}
R = \frac{1}{\Delta} \Big\{ &\Big[J_0\big(2\hat{\omega}\sqrt{\xi_2}\big) - iJ_1\big(2\hat{\omega}\sqrt{\xi_2}\big) \Big] \\
&\Big[Y_0\big(2\hat{\omega}\sqrt{\xi_1}\big) - iY_1\big(2\hat{\omega}\sqrt{\xi_1}\big) \Big] \cdot \\
&- \Big[J_0\big(2\hat{\omega}\sqrt{\xi_1}\big) - iJ_1\big(2\hat{\omega}\sqrt{\xi_1}\big) \Big] \\
&\Big[Y_0\big(2\hat{\omega}\sqrt{\xi_2}\big) - iY_1\big(2\hat{\omega}\sqrt{\xi_2}\big) \Big] \Big\},
\end{aligned}
\quad (16)
$$

$$
\begin{aligned}
T_r = \frac{2\,i}{\Delta} \Big[&J_1\big(2\hat{\omega}\sqrt{\xi_1}\big) Y_0\big(2\hat{\omega}\sqrt{\xi_1}\big) \\
&- J_0\big(2\hat{\omega}\sqrt{\xi_1}\big) Y_1\big(2\hat{\omega}\sqrt{\xi_1}\big) \Big],
\end{aligned}
\quad (17)
$$

$$
B_1 = -\frac{2\,i\,\hat{\omega}}{\Delta} \Big[Y_0\big(2\hat{\omega}\sqrt{\xi_1}\big) - iY_1\big(2\hat{\omega}\sqrt{\xi_1}\big) \Big],
\quad (18)
$$

$$
B_2 = \frac{2\,i\,\hat{\omega}}{\Delta} \Big[J_0\big(2\hat{\omega}\sqrt{\xi_1}\big) - iJ_1\big(2\hat{\omega}\sqrt{\xi_1}\big) \Big], \quad (19)
$$

where the determinant is:

$$
\begin{aligned}
\Delta = &\Big[J_0\big(2\hat{\omega}\sqrt{\xi_2}\big) + iJ_1\big(2\hat{\omega}\sqrt{\xi_2}\big) \Big] \\
&\Big[Y_0\big(2\hat{\omega}\sqrt{\xi_1}\big) - iY_1\big(2\hat{\omega}\sqrt{\xi_1}\big) \Big] \\
&- \Big[J_0\big(2\hat{\omega}\sqrt{\xi_1}\big) - iJ_1\big(2\hat{\omega}\sqrt{\xi_1}\big) \Big] \\
&\Big[Y_0\big(2\hat{\omega}\sqrt{\xi_2}\big) + iY_1\big(2\hat{\omega}\sqrt{\xi_2}\big) \Big].
\end{aligned}
\quad (20)
$$

Solutions (10)–(12) with the coefficients (16)–(19) are shown in Fig. 3 for $|\Phi(\xi)|$ (see line a). A wavy dependence of function $|\Phi(\xi)|$ in the region III is caused by bits of incident and reflected waves,
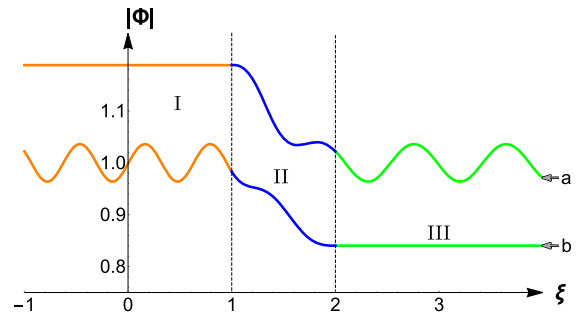
Figure 3
(Color figure online) Solutions for the free surface perturbation (10)–(12) with the coefficients (16)–(19) in terms of $|\Phi(\xi)|$. Line (**a**) pertains to the case when the incident wave arrives from the right where the depth $h_2 > h_1$, and line (**b**) pertains to the case when the incident wave arrives from the left where the depth $h_1 > h_2$. The Roman numerals correspond to the domains shown in Fig. 2

whereas in region I we have only one transmitted sinusoidal wave of a constant amplitude. Figure 4a shows the reflection coefficient and Fig. 4b the transmission coefficient as the functions of normalised frequency $\hat{\omega}$.

The plots shown in Figs. 3 and 4 were generated for the particular set of parameters with $h_1 = 1$ and $h_2 = 2$, and wave frequency $\hat{\omega} = 5$; for other parameters h_1, h_2, and $\hat{\omega}$ the plots are very similar to those shown in these figures.

In the limiting case $\hat{\omega} \to 0$ the formulae for the transformation coefficients reduce to the well-known expressions derived by Lamb (1932) for the step-wise bottom (see also Massel 1989; Kurkin et al. 2015 and references therein):

$$R = \frac{1 - \sqrt{k}}{1 + \sqrt{k}}, \quad T = \frac{2}{1 + \sqrt{k}}, \quad (21)$$

where $k = h_1/h_2$. Such reduction is quite natural, because in the limit $\hat{\omega} \to 0$ the wave lengths of scattered waves become much greater than the length of transient domain l_0.

The non-monotonic character of dependencies $|R|(\hat{\omega})$ and $|T|(\hat{\omega})$ is explained by the interference of waves within the transient zone $\xi_1 \le \xi \le \xi_2$ due to the reflections from the bottom edges at ξ_1 and ξ_2. However in the minima the reflection coefficient never vanishes (see Fig. 4), therefore the reflection-less propagation is impossible, although for some
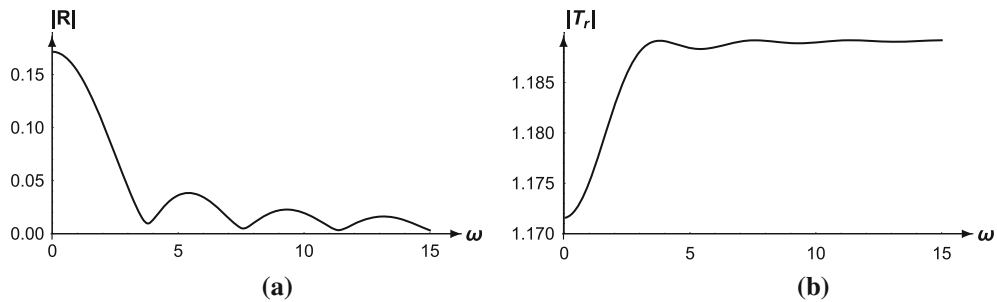
Figure 4

The reflection $|R|$ (**a**) and transmission $|T_r|$ (**b**) coefficients as the functions of normalised frequency $\hat{\omega}$ for the fixed value of $h_2/h_1 = 2$. The plots pertain to the case when the incident wave arrives from the right where the depth $h_2 > h_1$

"quasi-resonant" frequencies the reflected wave can be very small.

As follows from Fig. 4, the amplitude of a transmitted wave can be greater than the amplitude of an incident wave ($T > 1$); this is a usual effect when a wave travels from a deeper region to a shallower region, herewith its wavelength decreases and amplitude increases. The energy flux conserves in this case and results in the relationship between R, T, and $h_{1,2}$. The energy flux can be determined as the density of wave energy (which is proportional to the squared wave amplitude) times the group speed (see, e.g., Mei 1990; Dingemans 1997), which in the dimensionless variables for the shallow-water case is $c(\xi) = \sqrt{h(\xi)}$. Therefore, the energy flux conservation can be presented as:

$$c_1 T^2 = c_2(1 - R^2), \quad \text{or} \quad \sqrt{\frac{h_1}{h_2}} T^2 + R^2 = 1. \quad (22)$$

2.2. Wave Transformation in the Case of Increasing Depth

In this case when the incident wave arrives from the left we chose the coefficients of the system (10)–(12) as follows:

$$A_1 = 1, \quad A_2 = R, \quad C_1 = T_l, \quad C_2 = 0. \quad (23)$$

By substituting solutions (10)–(12) with the coefficients (23) into the boundary conditions (14), we obtain again for the transformation coefficients R and T_l, as well as for the amplitudes of waves in the transient domain 2 (see Fig. 2) B_1 and B_2:

$$R = \frac{1}{\Delta} \left\{ \left[J_0(2\hat{\omega}\sqrt{\xi_2}) + iJ_1(2\hat{\omega}\sqrt{\xi_2}) \right] \right.$$
$$\left[Y_0(2\hat{\omega}\sqrt{\xi_1}) + iY_1(2\hat{\omega}\sqrt{\xi_1}) \right].$$
$$- \left[J_0(2\hat{\omega}\sqrt{\xi_1}) + iJ_1(2\hat{\omega}\sqrt{\xi_1}) \right]$$
$$\left. \left[Y_0(2\hat{\omega}\sqrt{\xi_2}) + iY_1(2\hat{\omega}\sqrt{\xi_2}) \right] \right\}, \quad (24)$$

$$T_l = \frac{2i}{\Delta} \left[J_1(2\hat{\omega}\sqrt{\xi_2}) Y_0(2\hat{\omega}\sqrt{\xi_2}) \right.$$
$$\left. - J_0(2\hat{\omega}\sqrt{\xi_2}) Y_1(2\hat{\omega}\sqrt{\xi_2}) \right], \quad (25)$$

$$B_1 = \frac{2\hat{\omega}i}{\Delta} \left[Y_0(2\hat{\omega}\sqrt{\xi_2}) + iY_1(2\hat{\omega}\sqrt{\xi_2}) \right], \quad (26)$$

$$B_2 = -\frac{2\hat{\omega}i}{\Delta} \left[J_0(2\hat{\omega}\sqrt{\xi_2}) + iJ_1(2\hat{\omega}\sqrt{\xi_2}) \right], \quad (27)$$

where the determinant Δ is the same as in Eq. (20).

Solutions (10)–(12) with the coefficients (24)–(27) are shown in Fig. 3 for $|\Phi(\xi)|$ (see line b). Graphic of the reflection coefficient for the same depth ratio $h_2/h_1 = 2$ is the same as in Fig. 4a, and the graphic of transformation coefficient is similar to that shown in Fig. 4b, but with the additional multiplicative factor $\sqrt{h_2/h_1}$. Now the amplitude of transmitted wave is less than the amplitude of an incident wave ($T_l < 1$), but the energy flux still conserves and has the same form as in Eq. (22) with the depth interchange: $h_1 \longleftrightarrow h_2$. This is the direct consequence of the *reciprocity relationship* derived in (Mei 1990): $k_2 h_2 T_l = k_1 h_1 T_r$, where the wave numbers k_1 and k_2 are determined in Eq. (13).

3. The Piecewise-Quadratic Bottom Profile

In this section we consider the case when the the bottom profile in the transient domain between two semi-infinite intervals with a constant depth can be approximated by a smooth conjugation of two quadratic functions as shown in Fig. 5 by line 1. A similar problem was considered by Kajiura (1961) (see also Dingemans 1997) for the model when one quadratic function in the transient domain connects two bottom levels with the discontinuities of derivatives at the boundaries (see line 2 in Fig. 5). Kajiura derived the reflection coefficient by means of the JWKB method up to second order terms in the asymptotic expansion in small parameter $(kl_0)^{-1} \ll 1$, where k is the wave number and $l_0 = x_2 - x_1$ is the width of the transient domain. It has been shown that the reflection coefficient apart from an oscillatory structure of the dependence $R(\hat{\omega})$ has an asymptotic form $R \sim \hat{\omega}^{-1}$. This problem was reconsidered later by Mei (1990) who derived the exact solution for the transient domain with the quadratic bottom profile and obtained the transformation coefficients. Here we consider a similar problem, but with two quadratic functions representing smooth connection of two bottom levels as shown in Fig. 5. We show that the exact solutions can be constructed and the transformation coefficients can be derived in the analytic, although rather cumbersome form.

We assume that the bottom profile can be presented by two parabolic functions
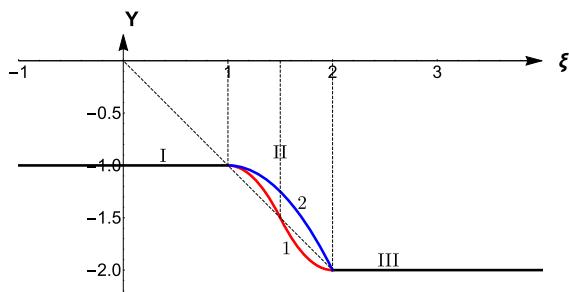
Figure 5

(Color figure online) A basin with the piecewise-quadratic bottom profile. Line 1 pertains to the case when two quadratic functions are conjugated at the middle of the transient zone ($\gamma = 0.5$—see the text) with smooth conjugation at the boundaries shown by dashed vertical lines. Line 2 pertains to the quadratic profile connecting two constant bottom levels as considered by Kajiura (1961) and Mei (1990)

$h(\xi) = a\xi^2 + b\xi + c$ with different coefficients smoothly matched with each other within the transient domain (at the point ξ_c) and with the constant bottom levels at the edges ξ_1 and ξ_2 of the transient domain. This can be achieved by the following choice of parabolic functions:

$$h_L(\xi) = \xi_1 + \frac{(\xi - \xi_1)^2}{\gamma(\xi_2 - \xi_1)}, \quad \xi_1 \le \xi \le \xi_c, \quad (28)$$

$$h_R(\xi) = \xi_2 - \frac{(\xi - \xi_2)^2}{(1 - \gamma)(\xi_2 - \xi_1)}, \quad \xi_c \le \xi \le \xi_2, \quad (29)$$

where $\xi_c = \xi_2\gamma + (1 - \gamma)\xi_1$ and $0 < \gamma < 1$. Varying the parameter γ one can obtain a class of smooth parabolic profiles connecting two constant bottom levels at different points; this can be treated as the spline approximation of a bottom profile. For simplicity we show in Fig. 5 only one such profile with $\gamma = 0.5$ (see line 1).

To construct a solution to the linearised set of Eqs. (4) and (5) it is convenient to reduce it to one equation for the perturbation of water surface $\eta(\xi, \tau)$:

$$\eta_{\tau\tau} - (\eta_\xi h)_\xi = 0 \quad (30)$$

Note that for the piecewise-quadratic bottom profile it is convenient to reduce the basic set of Eqs. (4) and (5) to one Eq. (30) for the surface elevation rather than to Eq. (6) for the fluid velocity, because the following Eq. (31) for function $\Phi \sim \eta$ reduces directly to the Legendre equation, whereas the governing Eq. (7) for function $\Psi \sim V$ reduces directly to the Bessel equation.

Substituting in Eq. (30) a solution in the form: $\eta(\xi, \tau) = e^{i\hat{\omega}\tau}\Phi(\xi)$ and the expressions for the bottom profile (28), (29), we obtain the Legendre equation for function $\Phi(\xi)$:

$$(a\xi^2 + b\xi + c)\Phi'' + (2a\xi + b)\Phi' + \hat{\omega}^2\Phi = 0, \quad (31)$$

where a, b, and c are some real constants. Solution to this equation can be expressed in general in terms of the linear combination of Legendre functions:

$$\Phi(\xi) = B_1 P_\nu^0\left(\frac{2a\xi + b}{\sqrt{b^2 - 4ac}}\right) + B_2 Q_\nu^0\left(\frac{2a\xi + b}{\sqrt{b^2 - 4ac}}\right), \quad (32)$$

where P_v^0 and Q_v^0 are the Legendre functions of the first and second kinds with $v = \left(\sqrt{1 - 4\hat{\omega}^2/a} - 1\right)/2$ (Polyanin and Zaitsev 2003), and B_1 and B_2 are arbitrary constants. In the particular case when $a = -\hat{\omega}^2/n(n+1)$, where n is a positive integer, one of these functions reduces to the Legendre polynomial $P_n(\xi)$.

Now solutions of Eq. (30) in all four domains shown in Fig. 5 can be presented as:

$$\Phi_l(\xi) = A_1 e^{-ik_1(\xi - \xi_1)} + A_2 e^{ik_1(\xi - \xi_1)}, \quad \xi \leq \xi_1, \quad (33)$$

$$\Phi_{p_1}(\xi) = B_1 \bar{w}_1 + B_2 \bar{w}_2, \quad \xi_1 \leq \xi \leq \xi_c, \quad (34)$$

$$\Phi_{p_2}(\xi) = C_1 \tilde{w}_1 + C_2 \tilde{w}_2, \quad \xi_c \leq \xi \leq \xi_2, \quad (35)$$

$$\Phi_r(\xi) = D_1 e^{-ik_2(\xi - \xi_2)} + D_2 e^{ik_2(\xi - \xi_2)}, \quad \xi \geq \xi_2, \quad (36)$$

where $A_{1,2}, B_{1,2}, C_{1,2}$ and $D_{1,2}$ are arbitrary constants,

$$\bar{w}_1 = P_v^0 \left[\frac{\xi - \xi_1}{\sqrt{\gamma \xi_1 (\xi_1 - \xi_2)}} \right], \quad \bar{w}_2 = Q_v^0 \left[\frac{\xi - \xi_1}{\sqrt{\gamma \xi_1 (\xi_1 - \xi_2)}} \right], \quad (37)$$

$$\tilde{w}_1 = P_\mu^0 \left[\frac{\xi - \xi_2}{\sqrt{(1 - \gamma) \xi_2 (\xi_2 - \xi_1)}} \right],$$
$$\tilde{w}_2 = Q_\mu^0 \left[\frac{\xi - \xi_2}{\sqrt{(1 - \gamma) \xi_2 (\xi_2 - \xi_1)}} \right], \quad (38)$$

and the indices v and μ are:

$$v = \frac{1}{2} \left[\sqrt{1 + 4\gamma \hat{\omega}^2 (\xi_1 - \xi_2)} - 1 \right],$$
$$\mu = \frac{1}{2} \left[\sqrt{1 + 4\hat{\omega}^2 (1 - \gamma)(\xi_2 - \xi_1)} - 1 \right]. \quad (39)$$

Solutions (33)–(36) can be matched at the boundaries of domains in the points $\xi = \xi_1, \xi_c$ and ξ_2 with the help of boundary conditions reflecting the continuity of function $\Phi(\xi)$ and its first derivative:

$$\Phi_l(\xi_1) = \Phi_{p_1}(\xi_1), \quad \Phi_{p_1}(\xi_c) = \Phi_{p_2}(\xi_c),$$
$$\Phi_{p_2}(\xi_2) = \Phi_r(\xi_2), \quad (40)$$

$$\Phi_l'(\xi_1) = \Phi_{p_1}'(\xi_1), \quad \Phi_{p_1}'(\xi_c) = \Phi_{p_2}'(\xi_c),$$
$$\Phi_{p_2}'(\xi_2) = \Phi_r'(\xi_2). \quad (41)$$

This gives a set of six linear algebraic equations for the coefficients $A_{1,2}, B_{1,2}, C_{1,2}$ and $D_{1,2}$.

Using these boundary conditions, we consider below surface wave transformation on the bottom unevenness when the incident wave arrives from the left and from the right. In the former case we set the following coefficients in the system (33)–(36):

$$A_1 = 0, \quad A_2 = T_l, \quad D_1 = R, \quad D_2 = 1 \quad (42)$$

and after that determine the transformation coefficients R, T_l, as well as $B_{1,2}$ and $C_{1,2}$. In the latter case we set the following coefficients in the system (33)–(36):

$$A_1 = 1, \quad A_2 = R, \quad D_1 = T_r, \quad D_2 = 0 \quad (43)$$

and determine the transformation coefficients R, T_r, as well as $B_{1,2}$ and $C_{1,2}$. Omitting long and tedious calculations, we obtain the transformation coefficients $R(\hat{\omega})$ and $T_{l,r}(\hat{\omega})$ which are shown in Fig. 6 for three values of γ: $\gamma = 0.1$ (line 1), $\gamma = 0.5$ (line 2), and $\gamma = 0.9$ (line 3). The reflection coefficients are again the same for the left- and right-propagating incident waves. The transmission coefficients are different as in the previous model with the piecewise-linear bottom profile, but proportional to each other, $|T_l| = |T_r| \sqrt{h_2/h_1}$, in accordance with the reciprocity theorem. Figure 6b shows the coefficient T_r as the function of normalised wave frequency for the same three values of γ: $\gamma = 0.1$ (line 1), $\gamma = 0.5$ (line 5), and $\gamma = 0.9$ (line 3).

We do not present here formulae for the coefficients $B_{1,2}$ and $C_{1,2}$, as well as the explicit solutions (33)–(36), because they look very cumbersome. However in Fig. 7 we illustrate solutions obtained in terms of $|\Phi(\xi)|$ for the particular wave frequency and depths h_1 and h_2.

In the limiting case $\hat{\omega} \to 0$ the formulae for the transformation coefficients reduce again to the well-known Lamb formulae for the step-wise bottom profile (21). The dependencies of transformation coefficients on frequency, $|R|(\hat{\omega})$ and $|T|(\hat{\omega})$, are still non-monotonic, but much smoother than in the former case of quasi-linear bottom profile (cf. graphics of Figs. 6 and 4), because in this case the bottom profile is much smoother having discontinuity only in the second derivative at the edge points ξ_1 and ξ_2. The energy flux conservation in the form of Eq. (22) has been tested and confirmed on the derived solutions.
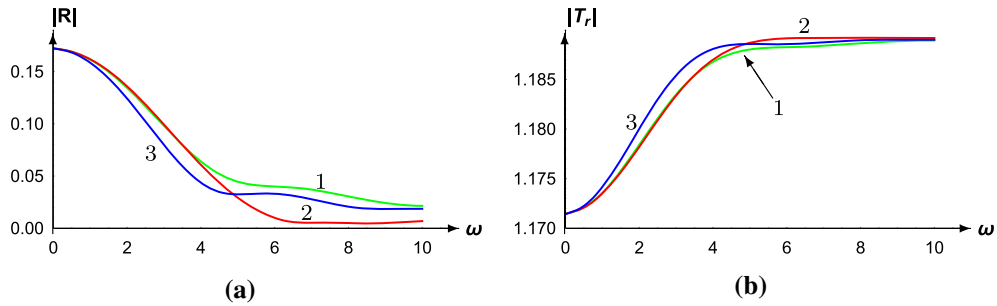
Figure 6
(Color figure online) The reflection R (frame a) and transmission T_r (frame b) coefficients as the functions of normalised frequency $\hat{\omega}$ for the fixed value of $h_2/h_1 = 2$ and $\hat{\omega} = 5$. Line 1 pertains to $\gamma = 0.5$, line 2—to $\gamma = 0.1$, and line 3—to $\gamma = 0.9$ (for the definition of γ see the text)
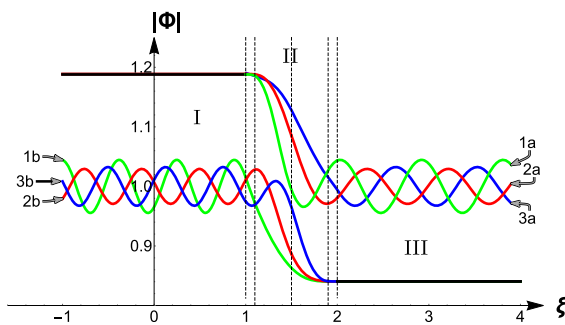
Figure 7
(Color figure online) Graphics of solutions for the free surface perturbation in terms of $|\Phi(\xi)|$. Lines 1a, 2a and 3a pertain to the case when the incident wave arrives from the right where the depth $h_2 > h_1$, and lines 1b, 2b and 3b pertain to the case when the incident wave arrives from the left where the depth $h_1 > h_2$. The numbers 1, 2, 3 correspond to the cases when $\gamma = 0.1, 0.5, 0.9$ respectively, and Roman numerals denote different spatial intervals as in Fig. 5. The plot was generated for the particular case when $h_1 = 1$ and $h_2 = 2$, and wave frequency $\hat{\omega} = 5$; for other parameters h_1, h_2, and $\hat{\omega}$ the plots are similar to these

4. Hyperbolic Tangent Bottom Profile

In this section we consider the bottom spatial variation that can be described by the tanh-function so that the fluid depth is: $h(\xi) = a\tanh(\xi) + b$, where $a = (h_2 - h_1)/2$ and $b = (h_2 + h_1)/2$. Figure 8 illustrates the tanh bottom profile (line 1) in comparison with the quadratic profile (line 2) and linear profile (dashed line) considered in the previous sections.

By substituting the depth profile into the equation for the velocity (6) we obtain:
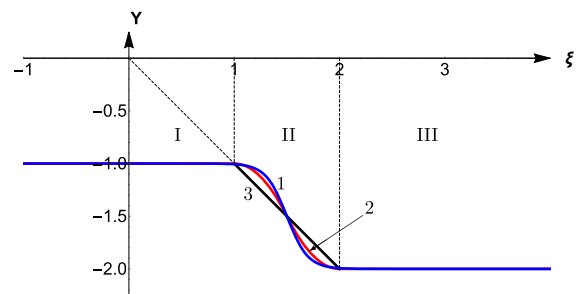
Figure 8
(Color figure online) The tanh bottom profile (line 1), combined quadratic profile (line 2) and linear profile (line 3). In the domains I and III the bottom quickly becomes constant, whereas in the domain II the bottom profile experiences a significant transition from one level to another level

$$[a\tanh(\xi) + b]\Psi_{\xi\xi} + 2a\mathrm{sech}^2(\xi)\Psi_\xi$$
$$+ \left[\hat{\omega}^2 - 2a\mathrm{sech}^2(\xi)\tanh(\xi)\right]\Psi = 0. \quad (44)$$

The solution to this equation can be presented in terms of hyper-geometric functions:

$$\Psi = \frac{(k^2-1)(1+\mathrm{e}^{2\xi})}{2(1+\mathrm{e}^{2\xi}k^2)}\mathrm{e}^{\mathrm{i}\tilde{\omega}(\xi-\mathrm{i}\pi/2)}$$
$$\times \left\{ C_1 \cdot {}_2F_1\left[\frac{\mathrm{i}(k-1)\tilde{\omega}}{2}, -\frac{\mathrm{i}(k+1)\tilde{\omega}}{2}, 1-\mathrm{i}\tilde{\omega}, -\frac{\mathrm{e}^{-2\xi}}{k^2}\right]\right.$$
$$+ C_2\left(\frac{\mathrm{e}^{-\xi+\mathrm{i}\pi/2}}{-k^2}\right)^{\mathrm{i}\tilde{\omega}}$$
$$\left.\times {}_2F_1\left[-\frac{\mathrm{i}(k-1)\tilde{\omega}}{2}, \frac{\mathrm{i}(k+1)\tilde{\omega}}{2}, 1+\mathrm{i}\tilde{\omega}, -\frac{\mathrm{e}^{-2\xi}}{k^2}\right]\right\},$$
$$(45)$$

where $k = \sqrt{h_2/h_1}$, $\tilde{\omega} = \hat{\omega}/\sqrt{h_2}$.

Substituting this solution into the Eq. (5), we obtain a solution for the perturbation of a free surface:

$$\Phi(\xi) = \frac{\sqrt{h_1}(k^2-1)e^{\pi/2}}{2}$$

$$\left(C_1 \left\{ {}_2F_1\left[\frac{i(k-1)\tilde{\omega}}{2}, -\frac{i(k+1)\tilde{\omega}}{2}, 1-i\tilde{\omega}, -\frac{e^{-2\xi}}{k^2}\right] \right. \right.$$

$$\left. - \frac{k+1}{k}{}_2F_1\left[\frac{i(k-1)\tilde{\omega}}{2}, 1-\frac{i(k+1)\tilde{\omega}}{2}, 1-i\tilde{\omega}, -\frac{e^{-2\xi}}{k^2}\right] \right\} e^{i\tilde{\omega}\xi}$$

$$- C_2 k^{-2i\tilde{\omega}} \left\{ {}_2F_1\left[-\frac{i(k-1)\tilde{\omega}}{2}, \frac{i(k+1)\tilde{\omega}}{2}, 1+i\tilde{\omega}, -\frac{e^{-2\xi}}{k^2}\right] \right.$$

$$\left. \left. - \frac{k+1}{k}{}_2F_1\left[-\frac{i(k-1)\tilde{\omega}}{2}, 1+\frac{i(k+1)\tilde{\omega}}{2}, 1+i\tilde{\omega}, -\frac{e^{-2\xi}}{k^2}\right] \right\} e^{-i\tilde{\omega}\xi} \right). \tag{46}$$

The asymptotics of this solution when $\xi \to \pm\infty$ are:

(1) $\xi \to +\infty$:

$$\Phi(\xi) = \frac{\sqrt{h_1}(k^2-1)}{2k}\left[-C_1 e^{i\tilde{\omega}(\xi-i\pi/2)} + C_2 k^{-2i\tilde{\omega}}e^{-i\tilde{\omega}(\xi-3i\pi/2)}\right], \tag{47}$$

(2) $\xi \to -\infty$:

$$\Phi(\xi) = k^{i(k-1)\tilde{\omega}}\sqrt{h_1}\Gamma(-ik\tilde{\omega})\left\{ C_2(k+1)\frac{\Gamma(i\tilde{\omega})}{\Gamma^2\left[-\frac{i(k-1)\tilde{\omega}}{2}\right]} \right.$$

$$- C_1(k-1)e^{2\pi\tilde{\omega}}\frac{\Gamma(-i\tilde{\omega})}{\Gamma^2\left[-\frac{i(k+1)\tilde{\omega}}{2}\right]} \right\} e^{i\tilde{\omega}(k\xi+3i\pi/2)}$$

$$+ k^{-i(k+1)\tilde{\omega}}\sqrt{h_1}\left\{ C_2(k-1)\frac{\Gamma(i\tilde{\omega})\Gamma(ik\tilde{\omega})}{\Gamma^2\left[\frac{i(1+k)\tilde{\omega}}{2}\right]} \right.$$

$$\left. - C_1 e^{2\pi\tilde{\omega}}\frac{k^2-1}{2k}\frac{\Gamma(-i\tilde{\omega})\Gamma(1+ik\tilde{\omega})}{\Gamma\left[\frac{i(k-1)\tilde{\omega}}{2}\right]\Gamma\left[1+\frac{i(k-1)\tilde{\omega}}{2}\right]} \right\} e^{-i\tilde{\omega}(k\xi-3i\pi/2)}. \tag{48}$$

Thus, one can see that asymptotically solution (46) represents oppositely travelling waves which can be presented in the form:

$$\Phi(\xi) = A_1 e^{i\tilde{\omega}\xi} + A_2 e^{-i\tilde{\omega}\xi}, \qquad \xi \to +\infty \tag{49}$$

$$\Phi(\xi) = B_1 e^{ik\tilde{\omega}\xi} + B_2 e^{-ik\tilde{\omega}\xi}, \qquad \xi \to -\infty, \tag{50}$$

where $A_{1,2}$ and $B_{1,2}$ are the coefficients in front of corresponding exponential functions in Eqs. (47) and (48).

Then, we can obtain the transformation coefficients of surface waves passing over such bottom unevenness. If an incident wave arrives from the right (from the deeper region as shown in Fig. 8), then we set:

$$A_1 = 1, \quad A_2 = R_r, \quad B_1 = T_r, \quad B_2 = 0 \tag{51}$$

and readily derive from Eqs. (47) and (48) the transformation coefficients:

$$R_r = -k^{-2i\tilde{\omega}}\frac{k+1}{k-1}\frac{\Gamma(-i\tilde{\omega})\Gamma^2\left[\frac{1}{2}i(k+1)\tilde{\omega}\right]}{\Gamma(i\tilde{\omega})\Gamma^2\left[\frac{1}{2}i(k-1)\tilde{\omega}\right]}, \tag{52}$$

$$T_r = k^{i(k-1)\tilde{\omega}}\frac{2k}{k+1}\frac{\Gamma(-i\tilde{\omega})\Gamma(-ik\tilde{\omega})}{\Gamma^2\left[-\frac{1}{2}i(1+k)\tilde{\omega}\right]}\frac{\sinh(\pi\tilde{\omega})\sinh(k\pi\tilde{\omega})}{\text{sech}^2\left[\frac{1}{2}(1+k)\pi\tilde{\omega}\right]}, \tag{53}$$

$$C_1 = \frac{-2e^{-\pi\tilde{\omega}/2}k}{\sqrt{h_1}(k^2-1)},$$

$$C_2 = \frac{-2e^{3\pi\tilde{\omega}/2}k}{\sqrt{h_1}(k-1)^2}\frac{\Gamma(-i\tilde{\omega})\Gamma^2\left[\frac{1}{2}i(k+1)\tilde{\omega}\right]}{\Gamma(i\tilde{\omega})\Gamma^2\left[\frac{1}{2}i(k-1)\tilde{\omega}\right]}. \tag{54}$$

If an incident wave arrives from the left (from the shallower region), then we set:

$$A_1 = 0, \quad A_2 = T_l, \quad B_1 = R_l, \quad B_2 = 1 \tag{55}$$

and readily derive again from Eqs. (47) and (48) the transformation coefficients:

$$R_l = -k^{4i\tilde{\omega}}R_r, \quad T_l = k^{i(k-1)\tilde{\omega}}\frac{k+1}{2k}\frac{\Gamma^2\left[\frac{1}{2}i(1+k)\tilde{\omega}\right]}{\Gamma(i\tilde{\omega})\Gamma(ik\tilde{\omega})}, \tag{56}$$

$$C_1 = 0, \quad C_2 = \frac{e^{\frac{3\pi\tilde{\omega}}{2}}k^{i(1+k)\tilde{\omega}}\Gamma^2\left[\frac{1}{2}i(1+k)\tilde{\omega}\right]}{\sqrt{h_1}(-1+k)\Gamma(i\tilde{\omega})\Gamma(ik\tilde{\omega})}. \tag{57}$$

Figure 9 illustrates solution (46) for the incident wave arriving from the right (line 1a) and from the left (line 1b) in comparison with the solutions derived for the piecewise-quadratic bottom profile (lines 2a and 2b correspondingly). As one can see from this figure, the spatial periods of bits are shorter in the case of tanh bottom profile, whereas their amplitudes are slightly greater than in the case of piecewise-quadratic bottom profile.

The moduli of transformation coefficients $|R_r|$ and $|T_r|$ are shown in Fig. 10 for the same two bottom profiles and for the case when the incident wave arrives from the right. In the case when the incident wave arrives from the left the modulus of reflection coefficient is the same as in the former case: $|R_l| = |R_r|$, and the transmission coefficient $|T_l|$ is related with the transmission coefficient $|T_r|$ by the reciprocity relationship: $|T_l| = |T_r|\sqrt{h_2/h_1}$.
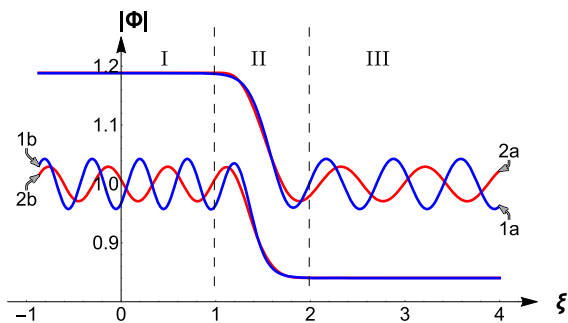
Figure 9

(Color figure online) Graphics of solutions for the free surface perturbation in terms of $|\Phi(\xi)|$ for the tanh bottom profile (lines 1a and 1b) and for the piecewise-quadratic bottom profile (lines 2a and 2b). Lines 1a and 2a pertain to incident waves arriving from the right, and lines 1b and 2b pertain to incident waves arrives from the left. The plot was generated for the particular case when $h_1 = 1$ and $h_2 = 2$, and wave frequency $\hat{\omega} = 5$; for other parameters h_1, h_2, and $\hat{\omega}$ the plots are similar to these

The general conclusion which follows from the comparison of transformation coefficients for all three cases of piecewise-linear, piecewise-quadratic, and tanh bottom profiles is that the smoother the profile, the smaller oscillations in the dependences of $|R(\hat{\omega})|$ and $|T(\hat{\omega})|$ (cf. lines 1 and 2 in Fig. 10 with the lines in Fig. 4). There are no oscillations in the dependencies $|R(\hat{\omega})|$ and $|T(\hat{\omega})|$ in the case of tanh-profile (see lines 1 in Fig. 10). In the case of piecewise-quadratic bottom profile the oscillations in such dependencies are very small and almost invisible (see lines 2 in Fig. 10), whereas in the case of piecewise-linear profile the oscillations are very well pronounced Fig. 4).

The conservation of energy flux in the form of Eq. (22) holds again, as expected.

Having solutions for the wave propagation over uneven bottom with the piecewise-linear, piecewise-quadratic, and tanh bottom profiles, we can solve problems with the more complicated bottom profiles, approximating them by sets of such functions for which exact solutions exist in the analytic forms. Below we present solutions for underwater trenches and barriers of different shapes. A similar problem was considered by Tokano (1960), Newman (1965), Kirby and Dalrymple (1983), Devillard et al. (1988) for a submerged rectangular bar and trench (see also Massel 1989 and Dingemans 1997 and references therein). In the paper by Rey et al. (1992) this problem was studied experimentally in the laboratory wave tank.

5. Wave Scattering on an Underwater Trench and Barrier with the Linear Slopes

Consider the bottom profiles shown in Fig. 11, which can be described by a set of linear functions $h(\xi) = a\xi + b$ with different parameters a and b. The left and right slopes of the trench/barrier can be described by the following parameters (see Fig. 11):

$$a_1 = \frac{h_2 - h_1}{\xi_2 - \xi_1}, \quad a_2 = \frac{h_2 - h_1}{\xi_3 - \xi_4}, \quad b_1 = \frac{h_1\xi_2 - h_2\xi_1}{\xi_2 - \xi_1},$$
$$b_2 = \frac{h_1\xi_3 - h_2\xi_4}{\xi_3 - \xi_4}.$$

(58)

Solutions in the each interval of the piecewise-linear bottom profile is:
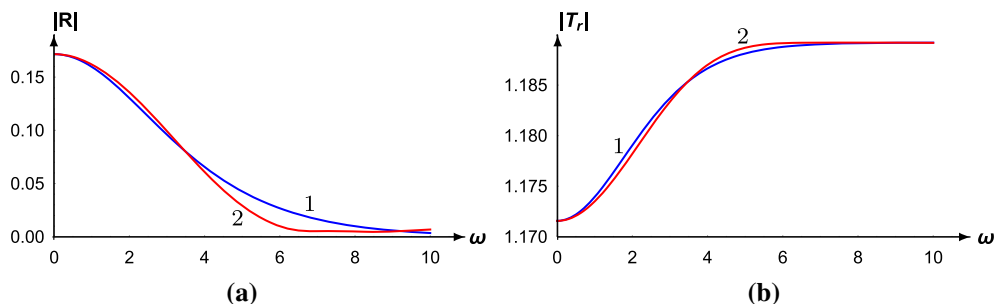
Figure 10

(Color figure online) The reflection (frame a) and transmission (frame b) coefficients for the tanh-profile (lines 1) and piecewise-quadratic (lines 2) bottom profile for the cases when the incident waves arrives from the right. The plots were generated for the particular case when $h_1 = 1$ and $h_2 = 2$, and wave frequency $\hat{\omega} = 5$
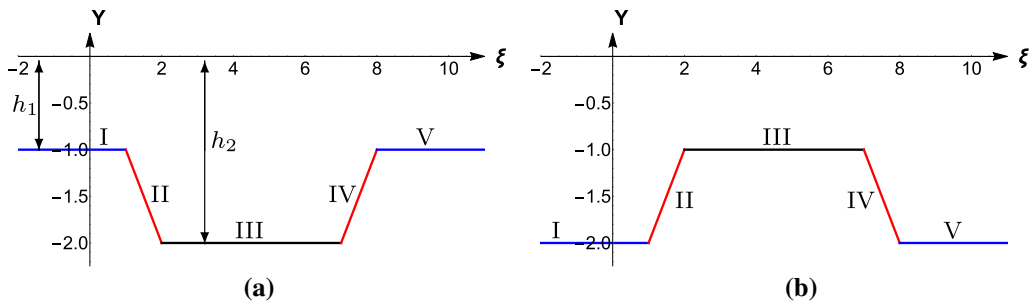
Figure 11
(Color figure online) Bottom profiles in the form of underwater trench (frame a) and barrier (frame b) with the linear slopes

$$\Phi_L = A_1 e^{-ik_1(\xi-\xi_1)} + A_2 e^{ik_1(\xi-\xi_1)}, \quad -\infty < \xi < \xi_1, \tag{59}$$

$$\Phi_{SL} = B_1 I_0\left(\frac{2i\omega}{a_1}\sqrt{a_1\xi+b_1}\right) + B_2 K_0\left(\frac{2i\omega}{a_1}\sqrt{a_1\xi+b_1}\right), \quad \xi_1 < \xi < \xi_2, \tag{60}$$

$$\Phi_C = C_1 e^{-ik_2\xi} + C_2 e^{i\xi_2 x}, \quad \xi_2 < \xi < \xi_3, \tag{61}$$

$$\Phi_{SR} = D_1 I_0\left(\frac{2i\omega}{a_2}\sqrt{a_2\xi+b_2}\right)$$
$$+ D_2 K_0\left(\frac{2i\omega}{a_2}\sqrt{a_2\xi+b_2}\right), \quad \xi_3 < \xi < \xi_4, \tag{62}$$

$$\Phi_R = E_1 e^{-ik_1(\xi-\xi_4)} + E_2 e^{i\xi_1(\xi-\xi_4)}, \quad \xi_4 < \xi < \infty. \tag{63}$$

When the incident wave propagates from the left to right in the geometry shown in Fig. 11, then we set the following coefficients $A_{1,2}$ and $E_{1,2}$:

$$A_1 = 1, \quad A_2 = R, \quad E_1 = T, \quad E_2 = 0. \tag{64}$$

To match solutions (59)–(63) at the points x_1, x_2, x_3, and x_4, we use eight boundary conditions which reflect continuations of function $\Phi(\xi)$ and its first derivative:

$$\Phi_L(\xi_1) = \Phi_{SL}(\xi_1), \quad \Phi_L'(\xi_1) = \Phi_{SL}'(\xi_1), \tag{65}$$

$$\Phi_{SL}(\xi_2) = \Phi_C(\xi_2), \quad \Phi_{SL}'(\xi_2) = \Phi_C'(\xi_2), \tag{66}$$

$$\Phi_C(\xi_3) = \Phi_{SR}(\xi_3), \quad \Phi_C'(\xi_3) = \Phi_{SR}'(\xi_3), \tag{67}$$

$$\Phi_{SR}(\xi_4) = \Phi_R(\xi_4), \quad \Phi_{SR}'(\xi_4) = \Phi_R'(\xi_4). \tag{68}$$

This leads to the set of eight linear algebraic equations for eight unknown coefficients R, T, $B_{1,2}$, $C_{1,2}$, and $E_{1,2}$. The set can be readily solved, but the solution looks very cumbersome, therefore we present below only a graphical illustration for the particular choices of parameters h_1, h_2, and $\hat{\omega} = 5$. Figure 12 shows wave filed amplitude $|\Phi(\xi)|$ for the trench with $h_2/h_1 = 2$ (frame a) and barrier with $h_1/h_2 = 2$ (frame b). In both cases it is supposed that the incident wave arrives from the left.

Figures 13 and 14 show the moduli of reflection and transmission coefficients respectively for the trench with $h_2/h_1 = 2$ (frames a) and barrier with $h_1/h_2 = 2$ (frames b). The oscillatory character of transformation coefficients as functions of wave frequency is the well-known phenomenon which has been noticed in many publications (see, e.g., Kajiura 1961; Massel 1989; Mei 1990; Dingemans 1997). The reason of this is the interference of standing waves within the trench or barrier.

In this section we have considered wave scattering on a symmetric trench or barrier; similarly one can consider a scattering on non-symmetric obstacles with the linear slopes or even more complicated piecewise-linear slopes.

6. Wave Scattering on an Underwater Trench and Barrier with the Piecewise-Quadratic Slopes

Consider now a wave scattering on the underwater obstacles (trench or barrier) when the left and right slopes can be described by a smooth conjugation of quadratic
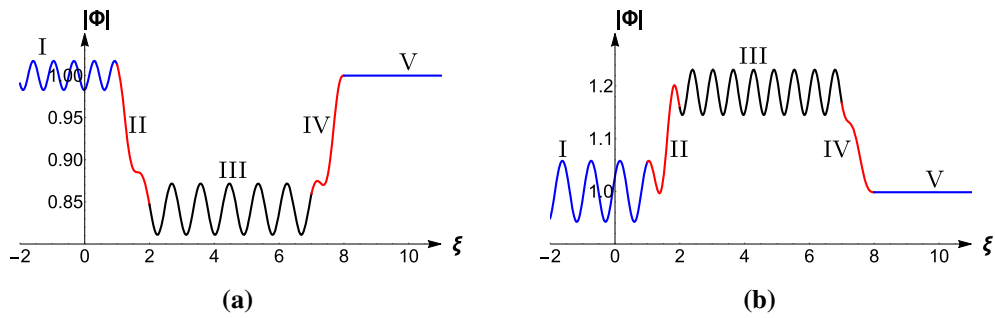
Figure 12
(Color figure online) Amplitude of surface wave field when an incident wave arrives from the left and scatters on the underwater trench $h_1 = 1$, $h_2 = 2$ (frame a) and barrier $h_1 = 2$, $h_2 = 1$ (frame b) with the linear slopes. In both cases the dimensionless frequency is $\hat{\omega} = 5$
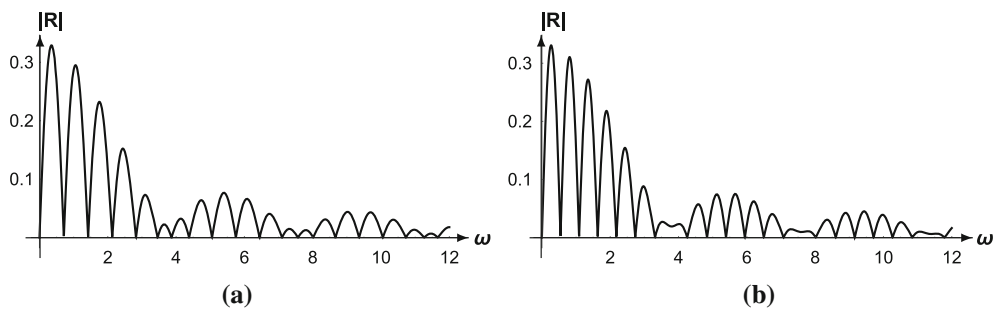
Figure 13
The moduli of reflection coefficients for a surface wave of dimensionless frequency $\hat{\omega} = 5$ scattering at the underwater trench (frames a) and barrier (frames b) with the linear slopes shown in Fig. 11
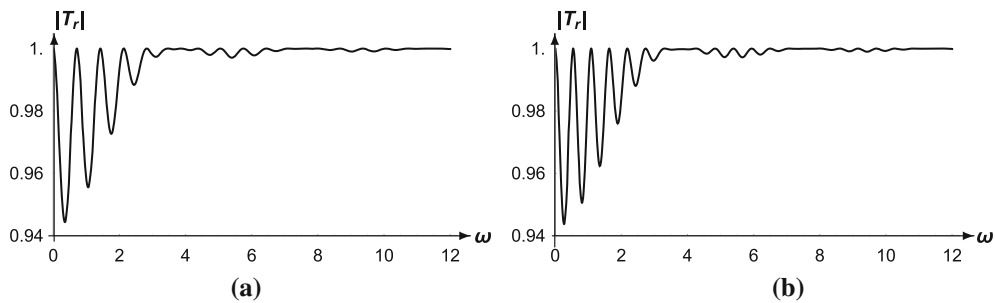
Figure 14
The moduli of transmission coefficients for a surface wave of dimensionless frequency $\hat{\omega} = 5$ scattering at the underwater trench (frames a) and barrier (frames b) with the linear slopes shown in Fig. 11

functions. The water depth over the uneven bottom in this case can be presented as $h(\xi) = a\xi^2 + b\xi + c$ (see Fig. 15). The basic differential equation for the free surface perturbation over the uneven bottom is:

$$\left(a\xi^2 + b\xi + c\right)\Phi''(\xi) + (2a\xi + b)\Phi'(\xi) + \omega^2\Phi(\xi) = 0. \tag{69}$$
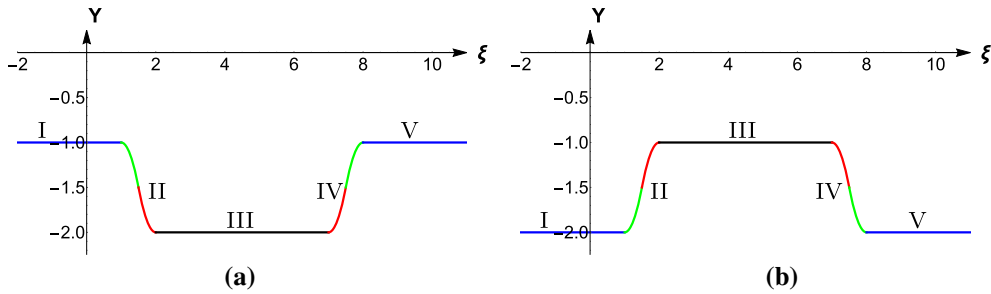
Figure 15

(Color figure online) Bottom profiles in the form of underwater trench (frame a) and barrier (frame b) with the piecewise-quadratic slopes

For the symmetric obstacles shown in Fig. 15 the coefficients of quadratic functions are:

$$a_1 = \frac{h_2 - h_1}{(\xi_2 - \xi_1)^2 \gamma}, \quad b_1 = \frac{2(h_1 - h_2)\xi_1}{(\xi_2 - \xi_1)^2 \gamma},$$

$$c_1 = h_1 + \frac{(h_2 - h_1)\xi_1^2}{(\xi_2 - \xi_1)^2 \gamma},$$

$$a_2 = \frac{h_2 - h_1}{(\xi_2 - \xi_1)^2(\gamma - 1)}, \quad b_2 = \frac{2(h_1 - h_2)\xi_2}{(\xi_2 - \xi_1)^2(\gamma - 1)},$$

$$c_2 = h_2 + \frac{(h_2 - h_1)\xi_2^2}{(\xi_2 - \xi_1)^2(\gamma - 1)},$$

$$a_3 = \frac{h_1 - h_2}{(\xi_3 - \xi_4)^2 \gamma}, \quad b_3 = \frac{2(h_2 - h_1)\xi_3}{(\xi_3 - \xi_4)^2 \gamma},$$

$$c_3 = h_2 + \frac{(h_1 - h_2)\xi_3^2}{(\xi_3 - \xi_4)^2 \gamma},$$

$$a_4 = \frac{h_1 - h_2}{(\xi_3 - \xi_4)^2(\gamma - 1)}, \quad b_4 = \frac{2(h_2 - h_1)\xi_4}{(\xi_3 - \xi_4)^2(\gamma - 1)},$$

$$c_4 = h_1 + \frac{(h_1 - h_2)\xi_4^2}{(\xi_3 - \xi_4)^2(\gamma - 1)}.$$

Here the parameter γ determines the positions of the conjugation of quadratic functions in the each slope:

$$\xi_{c1} = \xi_1 + \gamma(\xi_2 - \xi_1), \quad \xi_{c2} = \xi_3 + \gamma(\xi_4 - \xi_3). \tag{70}$$

Solutions to Eq. (69) can be presented in the dimensionless variables in terms of the Legendre polynomials $P_v(\xi)$ and $Q_v(\xi)$ [see Eqs. (34), (35)]:

$$\Phi(\xi) = B_1 P_v\left(\frac{2a\xi + b}{\sqrt{b^2 - 4ac}}\right) + B_2 Q_v\left(\frac{2a\xi + b}{\sqrt{b^2 - 4ac}}\right), \tag{71}$$

where $v = \left(\sqrt{1 - 4\hat{\omega}^2/a} - 1\right)/2$. Wave perturbations in each interval of ξ corresponding to different

domains of bottom profile (see Fig. 15) can be presented as follows:

$$\Phi_L(\xi) = A_1 e^{-ik_1(\xi - \xi_1)} + A_2 e^{ik_1(\xi - \xi_1)}, \quad -\infty < \xi < \xi_1,$$
$$\Phi_{SL1}(\xi) = B_1 P(a_1, b_1, c_1) + B_2 Q(a_1, b_1, c_1), \quad \xi_1 < \xi < \xi_{c1},$$
$$\Phi_{SL2}(\xi) = C_1 P(a_2, b_2, c_2) + C_2 Q(a_2, b_2, c_2), \quad \xi_{c1} < \xi < \xi_2,$$
$$\Phi_C(\xi) = D_1 e^{-ik_2 \xi} + D_2 e^{ik_2 \xi}, \quad \xi_2 < \xi < \xi_3,$$
$$\Phi_{SR1}(\xi) = E_1 P(a_3, b_3, c_3) + E_2 Q(a_3, b_3, c_3), \quad \xi_3 < \xi < \xi_{c2},$$
$$\Phi_{SR2}(\xi) = F_1 P(a_4, b_4, c_4) + F_2 Q(a_4, b_4, c_4), \quad \xi_{c2} < \xi < \xi_4,$$
$$\Phi_R(\xi) = G_1 e^{-ik_1(\xi - \xi_4)} + G_2 e^{ik_1(\xi - \xi_4)}, \quad \xi_4 < \xi < \infty.$$

To smoothly match these functions we use the boundary conditions of continuity of function $\Phi(\xi)$ and its first derivatives at the boundaries of intervals like in Eq. (14) above. As a result, we obtain a set of sixteen linear algebraic equations for the coefficients $A_{1,2}, B_{1,2}, \ldots, G_{1,2}$ that can be readily solved.

Figure 16 shows wave field amplitudes $|\Phi(\xi)|$ for the trench with $h_2/h_1 = 2$ (frame a) and barrier with $h_1/h_2 = 2$ (frame b). In both cases, it is assumed that the incident wave arrives from the left.

Figures 17 and 18 show the moduli of reflection and transmission coefficients respectively for the trench with $h_2/h_1 = 2$ (frames a) and barrier with $h_1/h_2 = 2$ (frames b).

It is interesting that in the case of an obstacle with the piecewise-quadratic slopes the number of resonances in the low-frequency domain is greater than in the case of an obstacle of the same width, but with the linear slopes (cf. Figs. 13, 14, 17 and 18). The basic features of transmission coefficients including maxima of reflection coefficients are similar in both cases.

In this section we considered again wave scattering on a symmetric trench or barrier; similarly one can consider a scattering on non-symmetric obstacles with the piecewise-quadratic slopes or even more
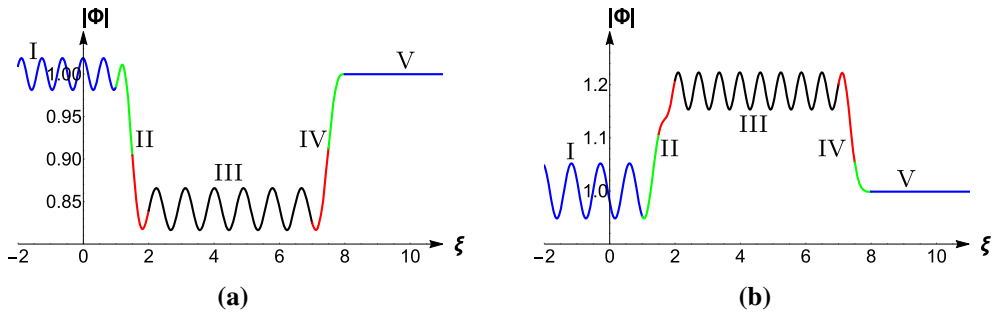
Figure 16

(Color figure online) Amplitude of surface wave field when an incident wave arrives from the left and scatters on the underwater trench $h_1 = 1$, $h_2 = 2$ (frame a) and barrier $h_1 = 2$, $h_2 = 1$ (frame b) with the piecewise-quadratic slopes (each segment consists of two different parabolic slopes). In both cases the dimensionless frequency is $\hat{\omega} = 5$
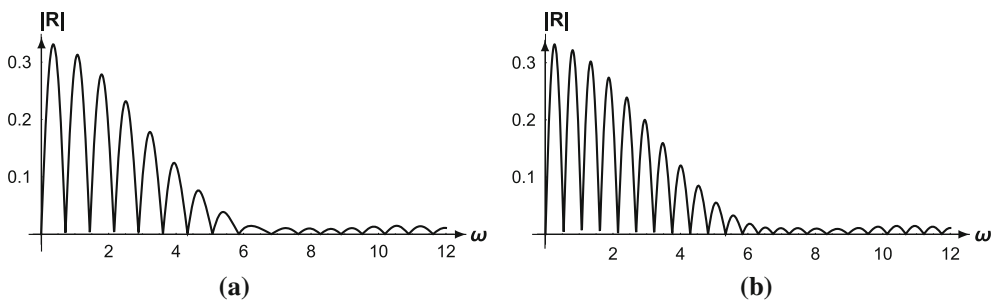
Figure 17

The moduli of reflection coefficients for a surface wave of dimensionless frequency $\hat{\omega} = 5$ scattering at the underwater trench (frames a) and barrier (frames b) with the piecewise-quadratic slopes shown in Fig. 15
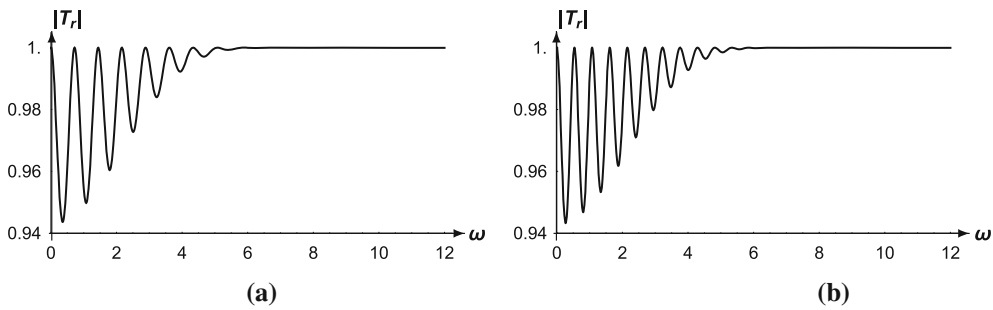
Figure 18

The moduli of transmission coefficients for a surface wave of dimensionless frequency $\hat{\omega} = 5$ scattering at the underwater trench (frames a) and barrier (frames b) with the piecewise-quadratic slopes shown in Fig. 15

complicated combination of piecewise-linear and piecewise-quadratic slopes. This opens a wide range of possibilities to approximate real bottom profiles with the set of such functions.

7. Wave Scattering on an Underwater Trench and Barrier with the Hyperbolic Tangent Profiles

In this section we consider wave transformation on the underwater obstacles with the slopes

describing by tanh-functions. We assume that the characteristic width of each slope l_0 is much less than the distance L between them. The bottom profiles for the trench and barrier are very similar to those shown in Fig. 15; they are practically indistinguishable from their counterparts described by piecewise-quadratic functions.

When the obstacle slopes are far enough from each other so that $L \gg l_0$, then the wave fields at the big distances from the slopes can be considered in the form of travelling waves in a fluid of constant depth. (Note that in the considered case, the characteristic width of function $\tanh(\xi)$ is one—see the beginning of Sect. 4). Here we consider for the sake of simplicity the situation when the characteristic width of an obstacle is much greater than the wavelength of an incident wave $L \gg \lambda$. However, there are no principal limitations for the exact solution in the case when $L \sim \lambda$. However, the problem of matching solutions in the vicinity of a transient zone $-L/2 \le \xi \le L/2$ makes the problem much more complicated and cumbersome.

For the left slopes of obstacles centred around $\xi = 0$, a solution to the wave equation has the following asymptotics:

$$\Phi_0(\xi) = w_1 e^{ik\hat{\omega}\xi} + w_2 e^{-ik\hat{\omega}\xi}, \quad \xi \to -\infty,$$
$$\Phi_0(\xi) = \tilde{w}_1 e^{i\hat{\omega}\xi} + \tilde{w}_2 e^{-i\hat{\omega}\xi}, \quad \xi \to +\infty$$

where

$$w_1 = e^{-\pi\hat{\omega}/2}\sqrt{h_1}k^{i(k-1)\hat{\omega}}\Gamma(-ik\hat{\omega})$$
$$\times \left\{ A_1 \frac{e^{\pi\hat{\omega}}(1-k)\Gamma(-i\hat{\omega})}{\Gamma^2\left[-\frac{1}{2}i(k+1)\hat{\omega}\right]} + A_2 \frac{e^{-\pi\hat{\omega}}(1+k)\Gamma(i\hat{\omega})}{\Gamma^2\left[-\frac{1}{2}i(k-1)\hat{\omega}\right]} \right\},$$

$$w_2 = e^{-\pi\hat{\omega}/2}\sqrt{h_1}k^{-i(k+1)\hat{\omega}}\Gamma(ik\hat{\omega})$$
$$\times \left\{ -A_1 \frac{e^{\pi\hat{\omega}}(1+k)\Gamma(-i\hat{\omega})}{\Gamma^2\left[\frac{1}{2}i(k-1)\hat{\omega}\right]} + A_2 \frac{e^{-\pi\hat{\omega}}(k-1)\Gamma(i\hat{\omega})}{\Gamma^2\left[\frac{1}{2}i(1+k)\hat{\omega}\right]} \right\},$$

$$\tilde{w}_1 = -\frac{A_1}{2k}\sqrt{h_1}(k^2-1)e^{\pi\hat{\omega}/2},$$

$$\tilde{w}_2 = \frac{A_2}{2}\sqrt{h_1}k^{-1-2i\hat{\omega}}(k^2-1)e^{-3\pi\hat{\omega}/2}.$$

The asymptotics of a solution to the wave equation for the second slope centred around $\xi = L$ is:

$$\Phi_0(\xi) == \hat{w}_1 e^{i\hat{\omega}\xi} + \hat{w}_2 e^{-i\hat{\omega}\xi}, \quad \xi \to -\infty,$$
$$\Phi_0(\xi) == \breve{w}_1 e^{ik\hat{\omega}\xi} + \breve{w}_2 e^{-ik\hat{\omega}\xi}, \quad \xi \to +\infty$$

whereFor the incident wave arriving from the left we set the following coefficients:

$$w_2 = 1, \quad w_1 = R, \quad \tilde{w}_1 = \breve{w}_1, \quad \tilde{w}_2 = \breve{w}_2,$$
$$\hat{w}_1 = 0, \quad \hat{w}_2 = T. \tag{72}$$

Then we can solve the set of equations for R, T, as well as $\tilde{w}_1$, $\tilde{w}_1$ and obtain:

$$\breve{w}_1 = e^{-iL\hat{\omega}-k\pi\hat{\omega}/2}\sqrt{h_1}k^{i(k-1)\hat{\omega}}\Gamma(-i\hat{\omega})$$
$$\times \left\{ B_1 \frac{e^{k\pi\hat{\omega}}(k-1)\Gamma(-ik\hat{\omega})}{\Gamma^2\left[-\frac{1}{2}i(k+1)\hat{\omega}\right]} + B_2 \frac{e^{-k\pi\hat{\omega}}(k+1)\Gamma(ik\hat{\omega})}{\Gamma^2\left[\frac{1}{2}i(k-1)\hat{\omega}\right]} \right\},$$

$$\breve{w}_2 = \frac{1}{2}e^{iL\hat{\omega}-k\pi\hat{\omega}/2}\sqrt{h_1}k^{i(k+1)\hat{\omega}}(k-1)$$
$$\times \left\{ B_1 \frac{e^{k\pi\hat{\omega}}(k+1)\Gamma(1+i\hat{\omega})\Gamma(-ik\hat{\omega})}{\Gamma\left[-\frac{1}{2}i(k-1)\hat{\omega}\right]\Gamma\left[1-\frac{1}{2}i(k-1)\hat{\omega}\right]} - B_2 \frac{2e^{-k\pi\hat{\omega}}\Gamma(i\hat{\omega})\Gamma(ik\hat{\omega})}{\Gamma^2\left[\frac{1}{2}i(k+1)\hat{\omega}\right]} \right\},$$

$$\hat{w}_1 = \frac{1}{2}B_1 e^{k(-iL+\pi/2)\hat{\omega}}\sqrt{h_1}(k^2-1),$$

$$\hat{w}_2 = -\frac{1}{2}B_2 e^{ikL\hat{\omega}-3k\pi\hat{\omega}/2}\sqrt{h_1}k^{2ik\hat{\omega}}(k^2-1).$$

$$R = \frac{4\pi^2}{\Delta_1} k^{2\mathrm{i}k\hat{\omega}} \Gamma(-\mathrm{i}k\hat{\omega})$$
$$\times \left\{ e^{2\mathrm{i}L\hat{\omega}}(k-1)^2 k^{\mathrm{i}(k+3)\hat{\omega}} \frac{\Gamma^2(\mathrm{i}\hat{\omega})\Gamma^4[\mathrm{i}(k-1)\hat{\omega}/2]}{\mathrm{sech}^2[(k+1)\pi\hat{\omega}/2]} \right.$$
$$\left. - k^{\mathrm{i}(k-1)\hat{\omega}}(k+1)^2 \frac{\Gamma^2(-\mathrm{i}\hat{\omega})\Gamma^4[\mathrm{i}(k+1)\hat{\omega}/2]}{\mathrm{sech}^2[(k-1)\pi\hat{\omega}/2]} \right\}, \tag{73}$$

$$T = \frac{(k^2-1)^2}{\Delta_2} e^{\mathrm{i}(k+1)L\hat{\omega}} k^{2\mathrm{i}(k+1)\hat{\omega}-1} \Gamma^4 \tag{74}$$
$$\left[\frac{\mathrm{i}}{2}(k-1)\hat{\omega}\right]\Gamma^4\left[\frac{\mathrm{i}}{2}(k+1)\hat{\omega}\right],$$

where

$$\Delta_1 = k^{\mathrm{i}\hat{\omega}}(k^2-1)e^{\mathrm{i}L\hat{\omega}}\hat{\omega}^2\Gamma(\mathrm{i}k\hat{\omega})\Gamma^2\left[-\frac{\mathrm{i}}{2}(k-1)\hat{\omega}\right]\Gamma^2\left[-\frac{\mathrm{i}}{2}(k+1)\hat{\omega}\right]$$
$$\times \left\{ k^{\mathrm{i}(k+2)\hat{\omega}}(k-1)^2 e^{\mathrm{i}L\hat{\omega}}\Gamma^2(\mathrm{i}\hat{\omega})\Gamma^4\left[\frac{\mathrm{i}}{2}(k-1)\hat{\omega}\right] \right.$$
$$\left. - k^{\mathrm{i}(k-2)\hat{\omega}}(k+1)^2 e^{-\mathrm{i}L\hat{\omega}}\Gamma^2(-\mathrm{i}\hat{\omega})\Gamma^4\left[\frac{\mathrm{i}}{2}(k+1)\hat{\omega}\right] \right\}$$
$$\Delta_2 = 4k^{2\mathrm{i}\hat{\omega}}e^{\mathrm{i}L\hat{\omega}}\Gamma^2(\mathrm{i}k\hat{\omega})\left\{ k^{2\mathrm{i}\hat{\omega}}e^{\mathrm{i}L\hat{\omega}}(k-1)^2\Gamma^2(\mathrm{i}\hat{\omega})\Gamma^4\left[\frac{\mathrm{i}}{2}(k-1)\hat{\omega}\right] \right.$$
$$\left. - k^{-2\mathrm{i}\hat{\omega}}e^{-\mathrm{i}L\hat{\omega}}(k+1)^2\Gamma^2(-\mathrm{i}\hat{\omega})\Gamma^4\left[\frac{\mathrm{i}}{2}(k+1)\hat{\omega}\right] \right\}. \tag{75}$$

The structures of the wave fields in terms of the dependencies $|\Phi(\xi)|$ for the trench with $h_2/h_1 = 2$ and barrier with $h_1/h_2 = 2$ are very similar to those shown in Fig. 16 for the piecewise-quadratic model. To minimise the number of illustrations, we do not present her the corresponding graphics. In Figs. 19 and 20 we show by lines 1 the moduli of reflection and transmission coefficients respectively for the trench with $h_2/h_1 = 2$ (frames a) and barrier with $h_1/h_2 = 2$ (frames b). For the comparison we show also by lines 2 similar coefficients derived in the previous Sect. 7 for the trench and barrier with the piecewise-quadratic slopes.

As one can see from these figures, the qualitative character of dependencies of transformation coefficients on frequency is similar. Moreover, even the maximum and minimum vales of transformation coefficients are the same. However, there are some differences. In particular, the number of significant maxima and minima in the low-frequency domain is greater in the case of obstacles with the tanh-slopes. And in this case the maxima of reflection coefficients decay slower with the frequency.

8. Conclusion

In this paper we have studied surface wave transformation on bottom unevenness in a shallow basin. We have obtained exact analytical solutions for three reference cases of (i) linearly increasing or decreasing bottom profiles on a finite spatial interval, (ii) piecewise-quadratic transient bottom profile between two constant values, and (iii) a transient bottom profile described by the tanh-function. We have studied also wave scattering on underwater barriers and trenches whose slopes can be described by the same functions (linear, piecewise-quadratic, and tanh-functions). The results obtained are in a good agreement with the results previously derived by different authors for the similar models (Kajiura
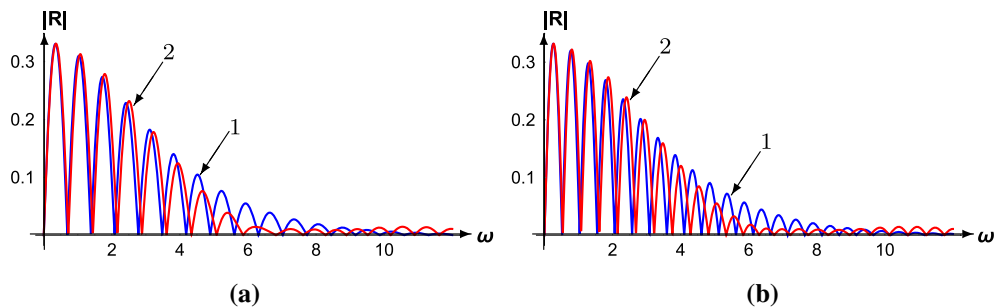
Figure 19

(Color figure online) The moduli of reflection coefficients for a surface wave of dimensionless frequency $\hat{\omega} = 5$ scattering at the underwater trench (frames **a**) and barrier (frames **b**). Lines 1 pertain to the obstacles with the tanh-slopes, and lines 2—to the obstacles with the piecewise-quadratic slopes shown in Fig. 15
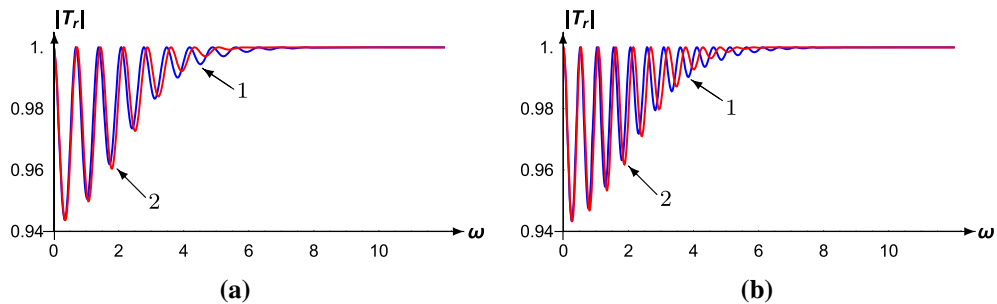
Figure 20

(Color figure online) The moduli of transmission coefficients for a surface wave of dimensionless frequency $\hat{\omega} = 5$ scattering at the underwater trench (frames **a**) and barrier (frames **b**). Lines 1 pertain to the obstacles with the tanh-slopes, and lines 2—to the obstacles with the piecewise-quadratic slopes shown in Fig. 15

1961; Dean 1964; Kirby and Dalrymple 1983; Massel 1989; Mei 1990; Dingemans 1997; Rey 1992; Rey et al. 1992; Kânoğlu and Synolakis 1998; Jung et al. 2008; Xie et al. 2011). In the limiting case when the wave frequency goes to zero we obtained the same transformation coefficients which are predicted by Lamb's theory (1932) for step-wise bottom.

In the meantime, there are some quantitative differences in the transformation coefficients for the different bottom profiles. In particular, the smoother the bottom profile is, the smoother the dependencies of transformation coefficients on frequency—cf. Figure 4 for the piecewise-linear profile with Fig. 6 for the piecewise-quadratic (line 2) and tanh (line 1) profiles. There are several well-pronounced oscillations in the dependence of $|R(\hat{\omega})|$ in Fig. 4. In particular, one can see that the reflection coefficient at some frequencies drops down to nearly zero. This provides almost reflectionless propagation (Didenkulova and Pelinovsky 2013, 2016) of an incident wave at the corresponding frequencies. We have tested the influence of basic parameters (the depth and frequency) on the structure of wave function $\Phi(\xi)$ and transformation coefficients. The results in all three model cases studied in the paper were qualitatively the same.

The situation is opposite for the wave scattering on underwater barriers or tranches. In particular, one can see fewer oscillations in the transformation coefficients shown in Figs. 13 and 14 for the barriers and tranches with the linear slopes in comparison with the barriers and tranches with the

piecewise-quadratic or tanh-slopes (cf. with Figs. 19 and 20).

More complicated real bottom profiles can be approximated with higher accuracy by the combination of those considered here: linear, quadratic, and tanh-profiles; such an approach has been exploited in Refs. Rey (1992), Rey et al. (1992), Kânoğlu and Synolakis (1998), Jung et al. (2008), Xie et al. (2011). The results obtained can be used, in particular, for the protection of beaches against storm surges, swells, and tsunami waves, as well as for the validation of numerical codes. On the basis of analytical results for the rather realistic bottom profiles, it would be of interest to analyse records of real tsunami waves passing over underwater obstacles of known profiles.

In conclusion, it is necessary to mention a further possible development of the results obtained in this paper. One of the obvious generalisations should take into account a finite spectrum of oceanic waves, whereas results presented in this paper pertain to a monochromatic wave. Then, we have studied here the normal incidence of a wave to the underwater obstacle, whereas oceanic waves can approach the coastal zone at an arbitrary angle. Therefore, the two-dimensional generalisation of the problems considered here seems to be reasonable. For some cases, such a problem has been studied both theoretically (Kirby and Dalrymple 1983; Kânoğlu and Synolakis 1998; Dingemans 1997) end experimentally (Thomson et al. 2007). The third generalisation is related to the finiteness of amplitude of real oceanic waves. In the coastal zones where the depth decreases, the

nonlinear effects become important. Therefore, it is topical to consider the nonlinear wave transformation on various bottom topography. Interesting exact solutions for the particular bottom profiles in the long-wave approximation were found in the papers (Mirchina and Pelinovski 1992; Pelinovsky 1996; Aksenov et al. 2018). Further efforts in the study of nonlinear effects in the coastal zones are highly desirable.

Acknowledgements

Publisher's Note Springer Nature remains neutral with regard to jurisdictional claims in published maps and institutional affiliations.

REFERENCES

Aksenov, A. V., Dobrokhotov, S. Y., & Druzhkov, K. P. (2018). Exact step-like solutions of one-dimensional shallow-water equations over a sloping bottom. *Mathematical Notes*, *104*, 915–921.

Belibassakis, K. A., Simon, B., Touboul, J., & Rey, V. (2017). A coupled-mode model for water wave scattering by vertically sheared currents in variable bathymetry regions. *Wave Motion*, *74*, 73–92.

Carrier, G. F., & Greenspan, H. P. (1958). Water waves of finite amplitude on a sloping beach. *Journal of Fluid Mechanics*, *4*, 97–109.

Dean, R. G. (1964). Long wave modification by linear transitions. *Journal of the Waterways, Harbors, and Coastal Engineering Division*, *90*, 1–29.

Devillard, P., Dunlop, F., & Souillard, B. (1988). Localization of gravity waves on a channel with random bottom. *Journal of Fluid Mechanics*, *186*, 521–538.

Didenkulova, I., & Pelinovsky, E. (2013). Analytical solutions for tsunami waves generated by submarine landslides in narrow bays and channels. *Pure and Applied Geophysics*, *170*(9–10), 1661–1671.

Didenkulova, I., & Pelinovsky, E. (2016). On shallow water rogue wave formation in strongly inhomogeneous channels. *Journal of Physics A: Mathematical and Theoretical*, *49*, 194001.

Dingemans, M. W. (1997). *Water wave propagation over uneven bottoms. Parts 1 and 2*. Singapore: World Scientific.

Ferrario, F., Beck, M. W., Storlazzi, C. D., Micheli, F., Shepard, C. C., & Airoldi, L. (2014). The effectiveness of coral reefs for coastal hazard risk reduction and adaptation. *Nature Communications*, *5*, 37–94.

Harris, D. L., & Vila-Concejo, A. (2013). Wave transformation on a coral reef rubble platform. *Journal of Coastal Research*, *65*, 506–510.

Jung, T.-H., Suh, K.-D., Lee, S. O., & Cho, Y.-S. (2008). Linear wave reflection by trench with various shapes. *Ocean Engineering*, *35*, 1226–1234.

Kajiura, K. (1961). On the partial reflection of water waves passing over a bottom of variable depth. In *Proceedings of the tsunami meetings, 10th Pacific Science Congress, IUGG Monograph* vol. 24 (pp. 206–234). Honolulu, Hawaii: University of Hawaii.

Kânoğlu, U., & Synolakis, C. E. (1998). Long wave runup on piecewise linear topographies. *Journal of Fluid Mechanics*, *374*, 1–28.

Kirby, J. T., & Dalrymple, R. A. (1983). Propagation of obliquely incident water waves over a trench. *Journal of Fluid Mechanics*, *133*, 47–63.

Kurkin, A. A., Semin, S. V., & Stepanyants, Y. A. (2015). Transformation of surface waves over a bottom step. *Izvestiya, Atmospheric and Oceanic Physics*, *51*(2), 214–223.

Lamb, H. (1932). *Hydrodynamics*. Cambridge: Cambridge University Press.

Levin, B. W., & Nosov, M. A. (2009). *Physics of tsunamis*. Berlin: Springer.

Massel, S. R. (1989). *Hydrodynamics of coastal zones*. Amsterdam: Elsevier.

Mei, C. C. (1990). Basic gravity wave theory. In J. B. Herbich (Ed.), *Handbook of coastal and ocean engineering vol. 1: Wave phenomena and coastal structures, chapter 1* (pp. 1–62). Houston: Gulf Publishing Company.

Mirchina, N. R., & Pelinovski, E. N. (1992). Nonlinear transformation of long waves at a bottom step. *Journal of Korean Society of Coastal and Ocean Engineers*, *4*(3), 161–167.

Newman, J. N. (1965). Propagation of water waves past long two-dimensional obstacles. *Journal of Fluid Mechanics*, *23*(1), 23–29.

Pelinovsky, E. N. (1996). *Tsunami wave hydrodynamics*. Nizhny Novgorod: Institute of Applied Physics of the Russian Academy of Sciences.

Polyanin, A. D., & Zaitsev, V. F. (2003). *Handbook of exact solutions for ordinary differential equations*. Boca Raton: Chapman and Hall/CRC.

Rey, V. (1992). Propagation and local behaviour of normally incident gravity waves over varying topography. *European Journal of Mechanics, B/Fluids*, *11*, 213–232.

Rey, V., Belzons, M., & Guazzelli, E. (1992). Propagation of surface gravity waves over a rectangular submerged bar. *Journal of Fluid Mechanics*, *235*, 453–479.

Sretenskii, L. N. (1977). *Theory of wave motions in a fluid*. Moscow: Nauka.

Stoker, J. J. (1957). *Water waves: The mathematical theory with applications*. Hoboken: Wiley.

Thomson, J., Elgar, S., Herbers, T. H. C., Raubenheimer, B., & Guza, R. T. (2007). Refraction and reflection of infragravity waves near submarine canyons. *Journal of Geophysical Research*, *112*, C10009.

Tokano, K. (1960). Effets d'un obstacle parallélépipedique sur la propagation de la houle. *La Houille Blanche*, *15*, 247–267.

Xie, J.-J., Liu, H.-W., & Li, P. (2011). Analytical solution for long-wave reflection by a rectangular obstacle with two scour trenches. *Journal of Engineering Mechanics*, *137*, 919–930.